

ELECTRONIC SUPPORTING INFORMATION

Co(II)-Based Single-Ion Magnets with 1,1'-ferrocenediyl-
bis(diphenylphosphine) metalloligands

J. Hrubý,^a D. Dvořák,^b L. Squillantini,^c M. Mannini,^c J. van Slageren,^d R. Herchel,^b I. Nemeč,^{a, b}
P. Neugebauer,^a*

^aCentral European Institute of Technology, CEITEC BUT, Purkyňova 656/123, 61200 Brno, Czech Republic

^bDepartment of Inorganic Chemistry, Faculty of Science, Palacký University, 17. listopadu 12, 77147 Olomouc, Czech Republic

^cDepartment of Chemistry "Ugo Schiff", University of Florence and INSTM Research Unit of Florence, via Lastruccia 3-13, 50019 Sesto Fiorentino, Italy

^dInstitute of Physical Chemistry, University of Stuttgart, Pfaffenwaldring 55, 70569 Stuttgart, Germany

This Supporting Information contains:

- 1) Crystallographic data
- 2) Temperature dependence in HF-ESR spectra
- 3) Static magnetic data measured for two batches of **3**
- 4) Dynamic magnetic properties at zero magnetic field
- 5) Debye's model parameters
- 6) CASSCF/NEVPT2 calculations comparison
- 7) Individual contributions to *D*-tensor
- 8) UV-VIS solution spectra comparison
- 9) XPS spectra comparison
- 10) XRPD data

1) Crystallographic data

Tab. S1 Crystallographic data for the reported compounds **1-3**.

	1	2	3
Formula	C ₃₄ H ₂₈ Cl ₂ Co ₁ Fe ₁ P ₂	C ₃₄ H ₂₈ Br ₂ Co ₁ Fe ₁ P ₂	C ₃₄ H ₂₈ Co ₁ Fe ₁ I ₂ P ₂
<i>M_r</i>	684.18	773.10	867.08
Crystal system	Triclinic, <i>P</i> $\bar{1}$	Triclinic, <i>P</i> $\bar{1}$	Monoclinic, <i>P</i> 2 ₁
<i>a</i> / Å	9.6088(6)	9.680(3)	8.9206(5)
<i>b</i> / Å	9.7213(6)	9.912(3)	18.0297(11)
<i>c</i> / Å	18.0783(10)	18.224(5)	9.9691(7)
α / °	96.099(5)	97.298(10)	90
β / °	99.950(5)	99.411(10)	94.857(2)
γ / °	115.437(6)	116.006(8)	90
<i>V</i> / Å ³	1470.81(17)	1511.0(7)	1597.63(17)
<i>Z</i>	2	2	2
<i>T</i> / K	150	150	150
<i>D_c</i> / g cm ⁻³	1.545	1.699	1.802
μ / mm ⁻¹	1.371	3.803	3.028
<i>F</i> (000)	698	770	842
Reflections collected/unique	5182/3995	5326/4641	10770/8825
Data/restraints/parameters	5182/0/361	5326/0/361	10770/1/361
Goodness-of-fit (GOF) on <i>F</i> ²	0.976	1.023	1.035
<i>R</i> ₁ , <i>wR</i> ₂ (<i>I</i> > 2σ(<i>I</i>)) ^{a, b}	0.0449/0.1153	0.0221/0.0447	0.0306/0.0517
<i>R</i> ₁ , <i>wR</i> ₂ (all data) ^{a, b}	0.0591/0.1191	0.0298/0.0461	0.0499/0.0644
CCDC number	1998989	1998990	1998991

$$^a R_1 = \frac{\sum(|F_o| - |F_c|)}{\sum|F_o|}, \quad ^b wR_2 = \left\{ \frac{\sum[w(F_o^2 - F_c^2)^2]}{\sum[w(F_o^2)^2]} \right\}^{1/2}$$

2) Temperature dependence in HF-ESR spectra

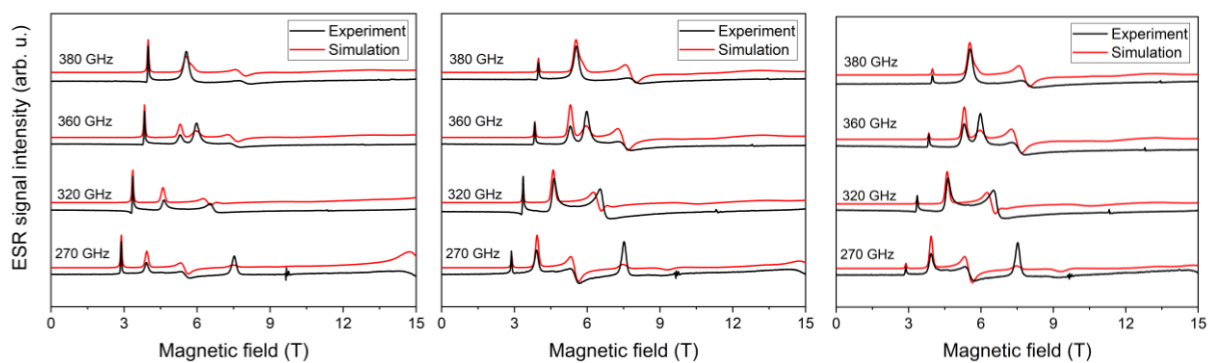


Fig. S1 HF-ESR spectra of **1** at 10 K (left), 20 K (middle), and 40 K (right). The black solid line represents experimental data and the red solid line is the simulation.

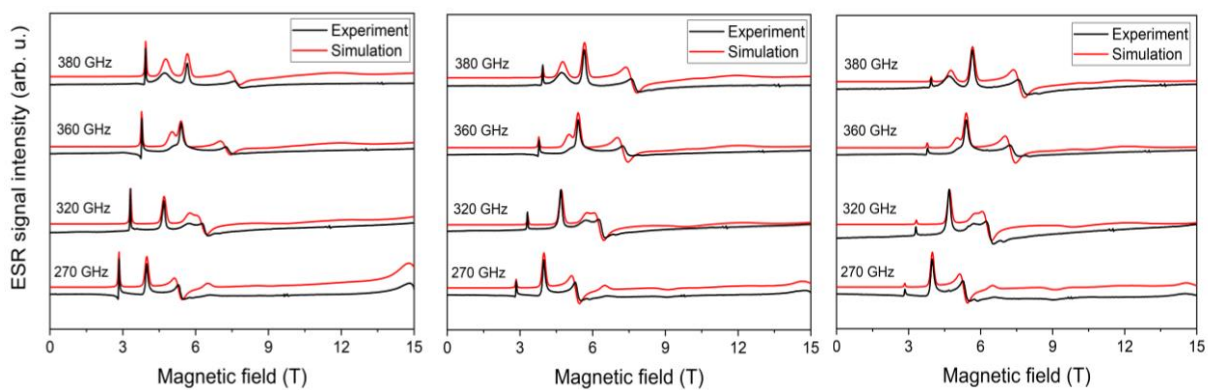


Fig. S2 HF-ESR spectra of **2** at 10 K (left), 20 K (middle), and 40 K (right). The black solid line represents experimental data and the red solid line is the simulation.

3) Static magnetic data measured for two batches of **3**

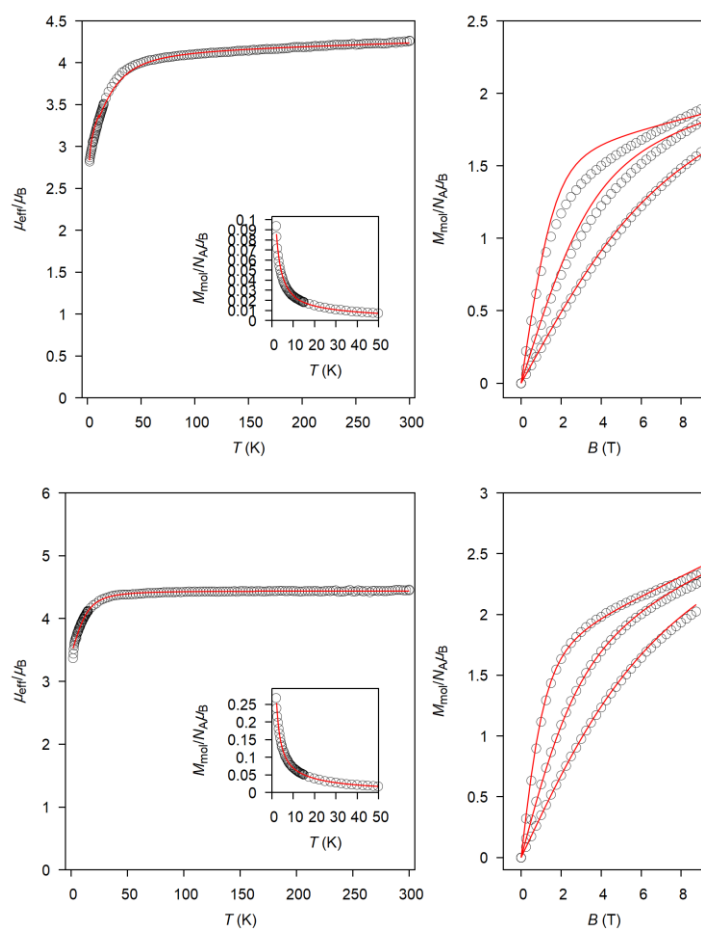


Fig. S3 Static magnetic data measured for two batches of **3**, batch 1 (top), batch 2 (bottom). Empty circles = experimental data, red line = fit with following results: batch 1, $g_{\text{iso}} = 2.133$, $D = -29.2 \text{ cm}^{-1}$, $E/D = 0$, $\chi_{\text{TIP}} = 4.949 \times 10^{-9} \text{ m}^3 \text{ mol}^{-1}$, $z_j = -0.326 \text{ cm}^{-1}$; batch 2, $g_{\text{iso}} = 2.291$, $D = -14.0 \text{ cm}^{-1}$, $E/D = 0$.

4) Dynamic magnetic properties at zero magnetic field

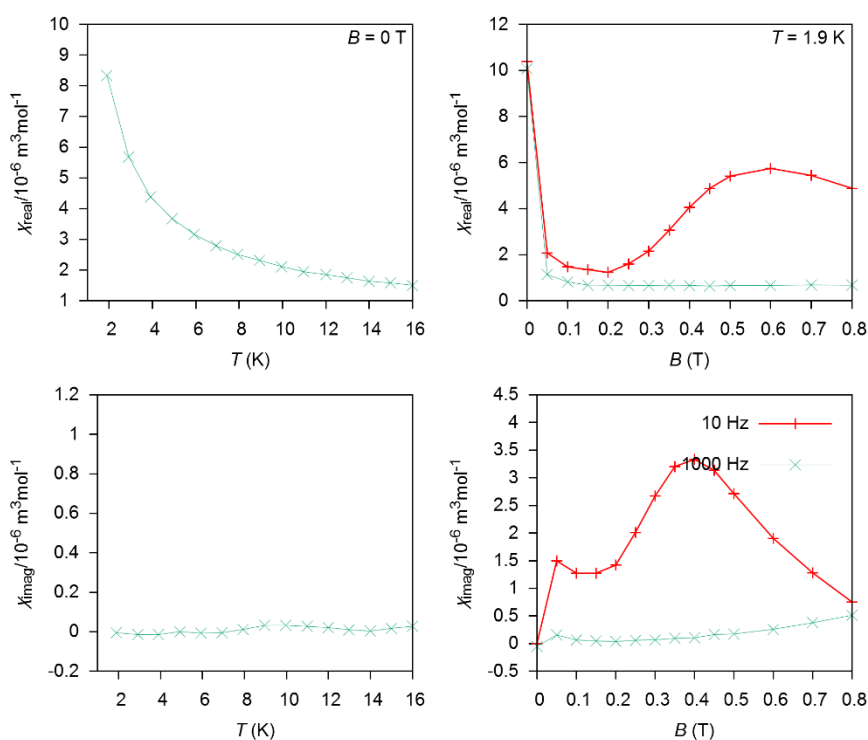


Fig. S4 In-phase χ_{real} and out-of-phase χ_{imag} molar susceptibilities for **1** at zero static magnetic field and in a non-zero static field. Lines serve as guides for the eyes.

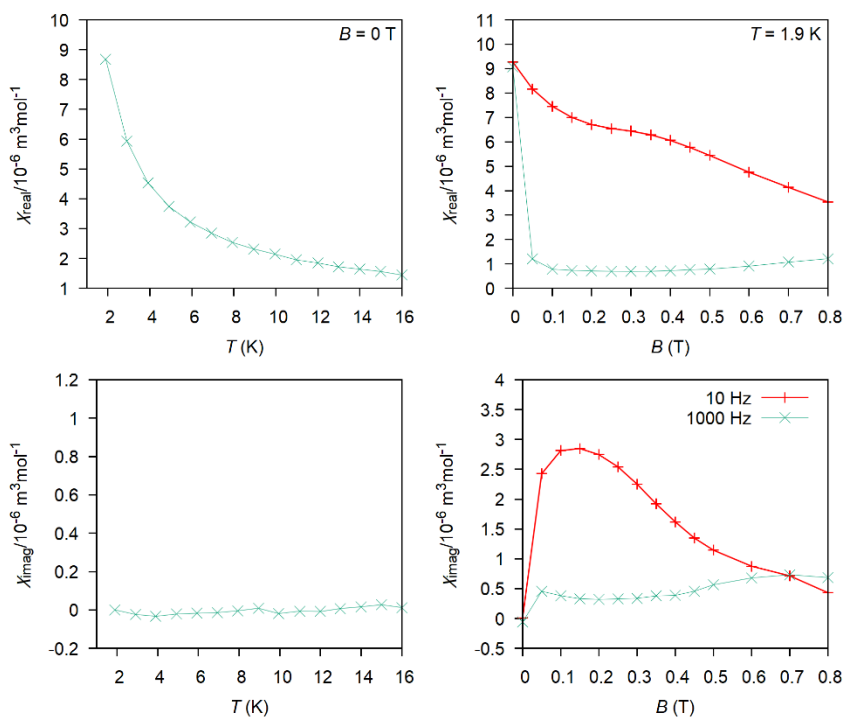


Fig. S5 In-phase χ_{real} and out-of-phase χ_{imag} molar susceptibilities for **2** at zero static magnetic field and in a non-zero static field. Lines serve as guides for the eyes.

5) One-component Debye's model parameters

Tab. S2 Parameters of one-component Debye model for **1** derived according to Eq. 4 in the main text.

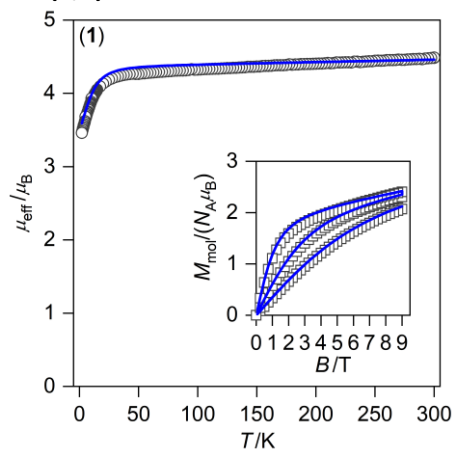
T/K	$\chi_s/(10^{-6} \text{ m}^3 \text{ mol}^{-1})$	$\chi_T/(10^{-6} \text{ m}^3 \text{ mol}^{-1})$	α	$\tau/(s)$
2.15	0.743	9.626	0.103	2.79E-02
2.40	0.699	8.508	0.086	5.48E-03
2.65	0.736	7.613	0.047	1.47E-03
2.90	0.807	7.083	0.047	5.07E-04
3.15	1.060	6.572	0.027	2.03E-04

Tab. S3 Parameters of one-component Debye model for **2** derived according to Eq. 4 in the main text.

T/K	$\chi_s/(10^{-6} \text{ m}^3 \text{ mol}^{-1})$	$\chi_T/(10^{-6} \text{ m}^3 \text{ mol}^{-1})$	α	$\tau/(s)$
1.90	0.672	9.399	0.166	6.46E-03
2.00	0.691	8.888	0.140	3.19E-03
2.10	0.722	8.439	0.125	1.62E-03
2.20	0.614	8.214	0.139	9.92E-04
2.30	0.429	7.863	0.154	4.94E-04
2.40	0.940	7.447	0.094	3.07E-04
2.50	0.863	7.172	0.096	1.78E-04
2.60	0.699	6.927	0.102	1.07E-04

6) CASSCF/NEVPT2 calculations comparison

CAS(7,5)



CAS(7,10)

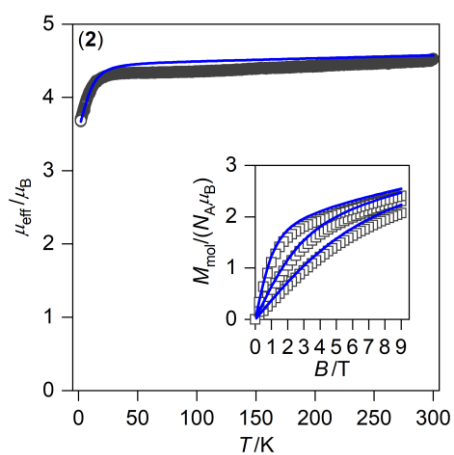
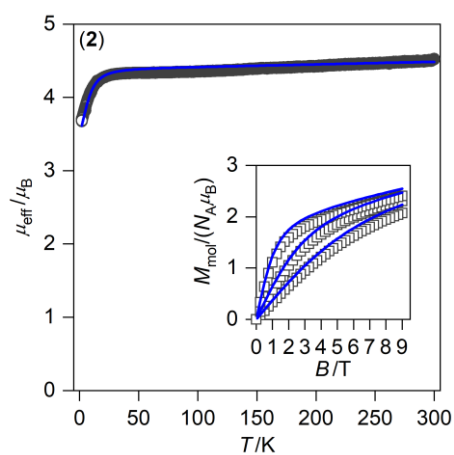
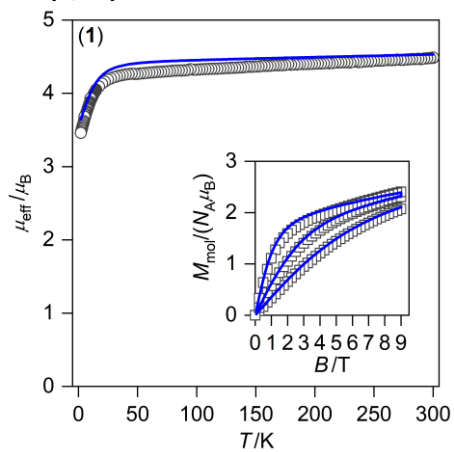


Fig. S6 Comparison of experimental magnetic data and the calculated magnetic data from CASSCF/NEVPT2 calculations.

7) Individual contributions to *D*-tensor

Tab S4. Individual contributions to *D*-tensor for **1-3** calculated by CASSCF/NEVPT2 with CAS(7,5).

(2S+1)	Root	1		2		3	
		<i>D</i>	<i>E</i>	<i>D</i>	<i>E</i>	<i>D</i>	<i>E</i>
4	0	0.000	0.000	-0.000	0.000	0.000	-0.000
4	1	-20.813	-20.813	-11.591	0.494	-15.630	-2.237
4	2	6.113	6.113	-0.057	4.139	6.562	-8.638
4	3	9.722	9.722	10.101	-5.864	11.402	11.211
4	4	-6.896	-6.896	-7.898	0.171	-8.288	-0.655
4	5	-0.085	-0.085	-0.289	0.031	-0.525	-0.001
4	6	0.017	0.017	0.037	-0.008	0.041	-0.039
4	7	0.006	0.006	0.012	-0.001	0.011	-0.011
4	8	0.000	0.000	0.001	0.000	-0.003	-0.001
4	9	-0.015	-0.015	-0.024	0.000	-0.028	-0.000
2	0	-1.028	-1.028	-0.462	0.501	-0.655	-0.274
2	1	-0.371	-0.371	-0.752	-0.660	-0.837	0.899
2	2	-0.005	-0.005	0.003	0.000	0.176	-0.001
2	3	0.112	0.112	0.113	0.000	0.015	0.000
2	4	0.110	0.110	0.106	0.015	0.121	-0.000
2	5	0.002	0.002	-0.007	0.004	-0.043	-0.039
2	6	2.401	2.401	-0.827	-0.541	0.058	1.554
2	7	-2.079	-2.079	1.801	-0.470	0.998	0.846
2	8	-2.484	-2.484	-2.286	0.648	-2.431	-2.441
2	9	0.837	0.837	0.499	-0.007	-0.004	0.005
2	10	-0.162	-0.162	-0.042	-0.048	0.215	0.047
2	11	-0.090	-0.090	-0.033	-0.035	0.010	0.154
2	12	-0.004	-0.004	0.034	0.007	0.389	-0.005
2	13	0.081	0.081	0.140	0.025	0.084	0.114
2	14	-0.012	-0.012	-0.007	0.006	-0.021	-0.020
2	15	-0.057	-0.057	0.149	-0.002	0.118	0.001
2	16	-0.061	-0.061	-0.125	0.067	-0.021	-0.030
2	17	0.166	0.166	-0.008	0.048	-0.167	-0.156
2	18	-0.058	-0.058	-0.048	-0.005	-0.015	-0.016
2	19	-0.035	-0.035	-0.065	-0.015	-0.151	0.198
2	20	-0.022	-0.022	-0.024	0.008	-0.009	0.012
2	21	-0.058	-0.058	-0.030	-0.016	-0.012	0.021
2	22	-0.430	-0.430	-0.007	-0.032	-0.004	0.003
2	23	0.038	0.038	-0.512	-0.246	-0.582	0.607
2	24	-0.500	-0.500	-0.521	0.254	-0.581	-0.596
2	25	0.916	0.916	1.153	0.030	1.212	0.007
2	26	-0.001	-0.001	-0.002	0.002	-0.000	-0.000
2	27	0.002	0.002	0.003	-0.000	0.003	-0.000
2	28	-0.000	-0.000	-0.000	-0.000	-0.001	-0.000
2	29	-0.070	-0.070	-0.020	0.006	-0.121	-0.048
2	30	0.033	0.033	-0.061	-0.016	0.080	-0.008
2	31	0.068	0.068	0.132	0.030	0.104	0.025
2	32	0.084	0.084	0.050	-0.001	0.027	0.005
2	33	0.006	0.006	-0.002	0.001	0.001	-0.000
2	34	0.000	0.000	0.001	0.000	0.000	0.000
2	35	-0.006	-0.006	-0.001	0.001	0.000	-0.000
2	36	-0.002	-0.002	-0.003	-0.002	-0.000	-0.000
2	37	0.006	0.006	-0.001	0.004	-0.010	-0.009
2	38	-0.014	-0.014	-0.013	-0.004	-0.009	-0.015
2	39	-0.043	-0.043	-0.026	-0.009	-0.029	0.041

8) UV-VIS solution spectra comparison

Fig. S7 shows UV-VIS solution spectra of dissolved **1** and **2** in 1 mM dichloromethane. The peaks in **Tab. S5** agreed with the previous study.¹ They showed a slightly detectable band at around 480 nm which can be ascribed to the $e_2 - e_1$ transition in the ferrocenyl moiety. In addition to this band, several other peaks observed can be assigned to d-d transitions of the $3d^7$ central ion in the approximately tetrahedral ligand field.² $[\text{CoBr}_2(\text{dppf})]$ peaks were shifted towards higher wavelengths, which can be attributed to the presence of bromide ligand instead of chloride.

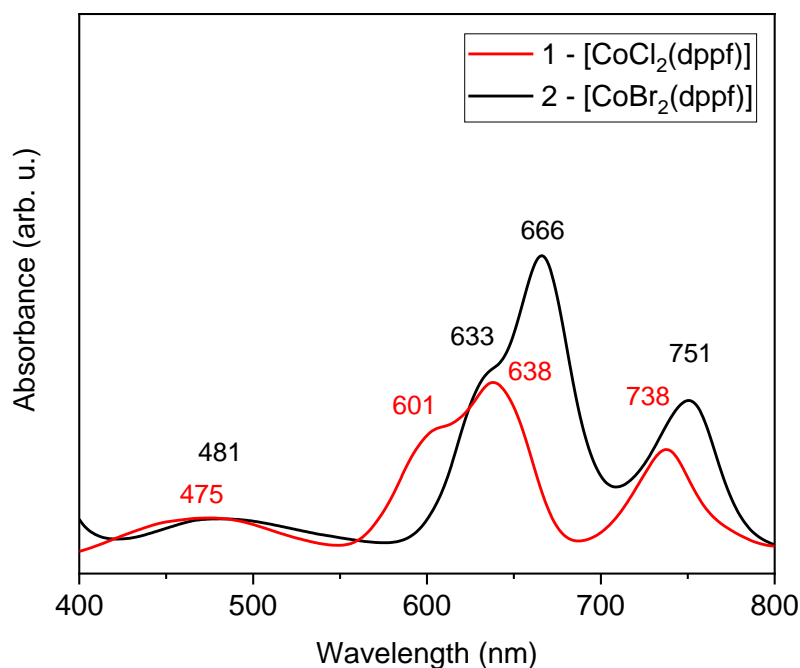


Fig. S7 UV-VIS spectra for compound **1** (red line) and **2** (black line) in 1 mM dichloromethane solution.

Tab. S5. UV-VIS spectra peak positions with literature comparison.

Complex	λ_{max} (nm)				Source
1a - $[\text{CoCl}_2(\text{dppf})]$	475	601	638	738	This Work
1b - $[\text{CoCl}_2(\text{dppf})]$	450	606	636	737	Ref. ¹
2 - $[\text{CoBr}_2(\text{dppf})]$	481	633	666	751	This Work

*In CH_2Cl_2 at 25 °C.

9) XPS spectra comparison

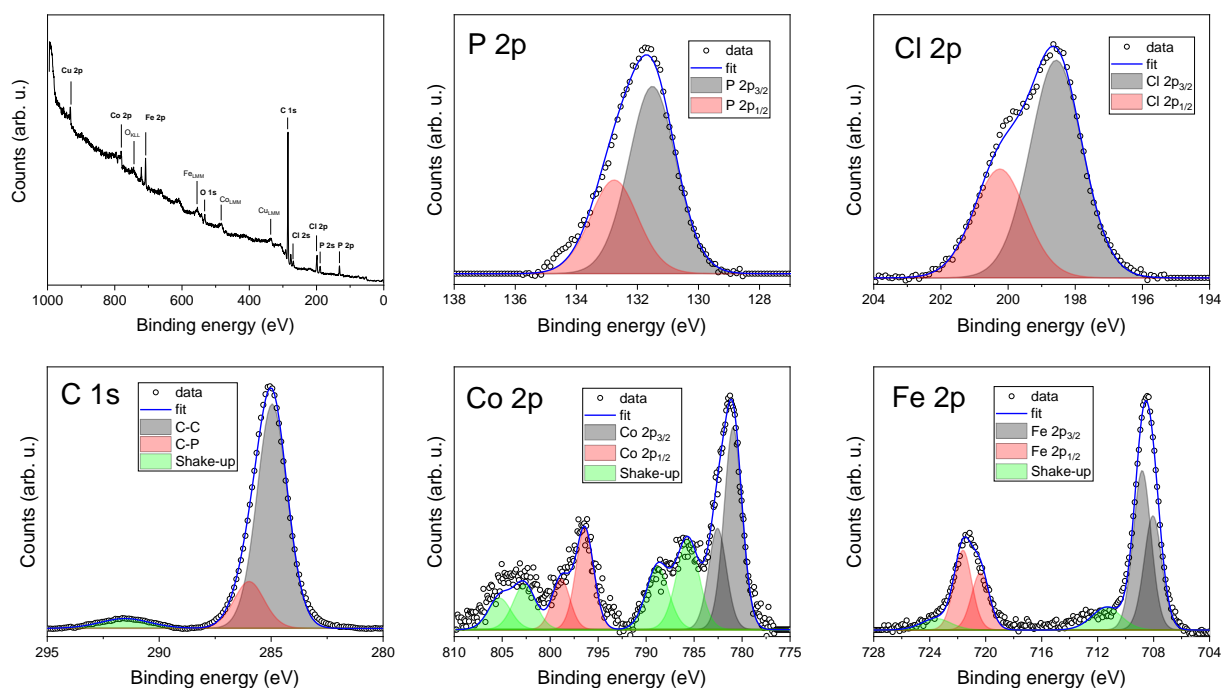


Fig. S8 XPS spectra for bulk compound **1**, survey (top left), and then according to elements, spectra for P 2p, Cl 2p, C 1s, Co 2p, and Fe 2p photoelectron peaks.

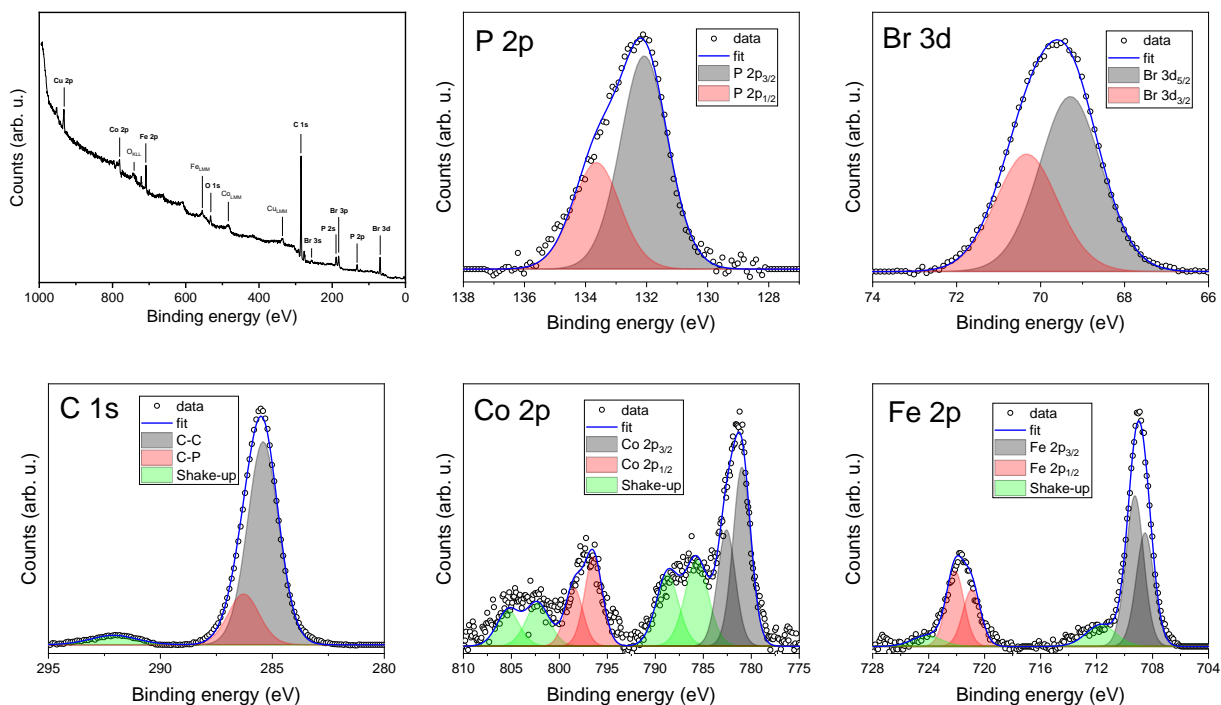


Fig. S9 XPS spectra for bulk compound **2**, survey (top left), and then according to elements, spectra for P 2p, Br 3d, C 1s, Co 2p, and Fe 2p photoelectron peaks.

The chemical composition of bulk **1** and **2** was probed by means of XPS. **Fig. S8** shows the survey spectrum which exhibited O 1s, C 1s, P 2s, P 2p, Cu 2p, Cl 2s, Cl 2p, Fe 2p, and Co 2p photoelectron peaks. In the case of **2**, Br 3d instead of Cl 2p was present in **Fig. S9**. Both spectra showed also visible O_{KLL}, Fe_{LMM}, Co_{LMM}, Cu_{LMM} Auger peaks. Highly resolved spectra of C 1s, P 2p, Cl 2p (or Br 3d), Co 2p, and Fe 2p for both compounds revealed a similar chemical environment, through a fitting process by utilising the convolution of Voigt curves to reproduce spectra. The best-fit parameters were found by applying constraints to the components forming the overall spectrum based on the nature of the systems: taking into account the relationship between components area and total angular momentum multiplicity of the final states (for spectra related to orbitals with non-zero angular momentum) and assuming the same FWHM for analogues components in each sample.^{3,4} XPS spectra of bulk **2** exhibited main ferrocene peak Fe 2p_{3/2} at 708.5 eV with spin-orbit coupling (SOC) separation of 12.4 eV, which is in agreement with previous studies.⁵⁻⁷ The Co 2p photoemission line Co 2p_{3/2} at 780.9 eV with SOC of 15.4 eV. Both compounds **1** and **2** exhibit shake-up features, which serve as a fingerprint of having paramagnetic Co(II) complex in the high-spin state.⁸⁻¹¹

Fig. S10 shows XPS survey spectra for bulk powder scratched on Cu foil (bulk), drop-cast from a 5 mM solution on Au(111) in a nitrogen atmosphere (drop), and a sublimated 30 nm thick film on Au(111) substrate (subl).

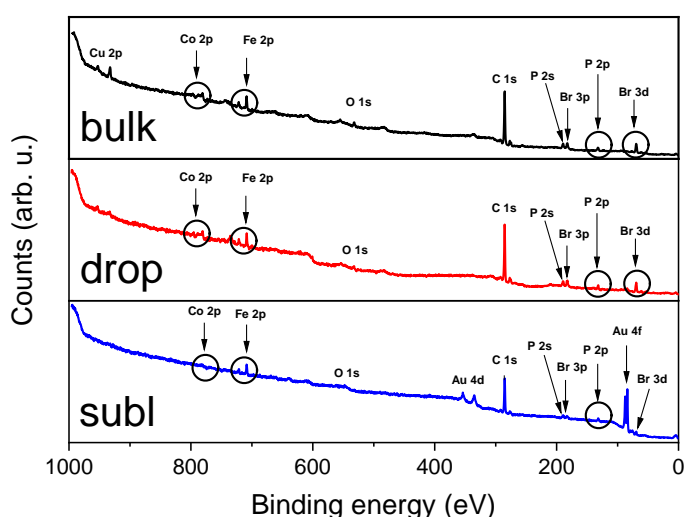


Fig. S10 XPS survey spectra of **2** as a bulk powder (top), drop-cast in nitrogen on Au(111) (middle), and sublimated on Au(111).

Tab. S6 shows a comparison of Fe 2p_{3/2} and Co 2p_{3/2} peak binding energies with previous studies. For cobalt, a slight shift (0.8 eV) of the 2p_{3/2} peak has been observed between the sublimated sample and bulk powder. Considering the direction of the shift (toward lower binding energies), the bromine deficiency, the excess of phosphorous and iron evidenced from stoichiometry evaluations, one scenario might be the partial decomposition of [CoBr₂(dppf)]. However, Co 2p_{3/2} peak positions are in a good agreement with similar systems reported in the literature, with slight shifts due to the differences in the coordination environment.

Tab. S6 Positions of Fe 2p_{3/2} and Co 2p_{3/2} binding energies.

	Fe 2p _{3/2}	Co 2p _{3/2}
Bulk	708.5	781.0
Drop	708.3	780.6
Subl	708.4	780.2
Reference	708.5 ¹² , 708.1 ¹³ , 707.9 ¹⁴ , 708.0 ⁶	780.1 ¹⁵ , 780.9 ¹⁶ , 781.2 ¹⁶

10) XRPD data

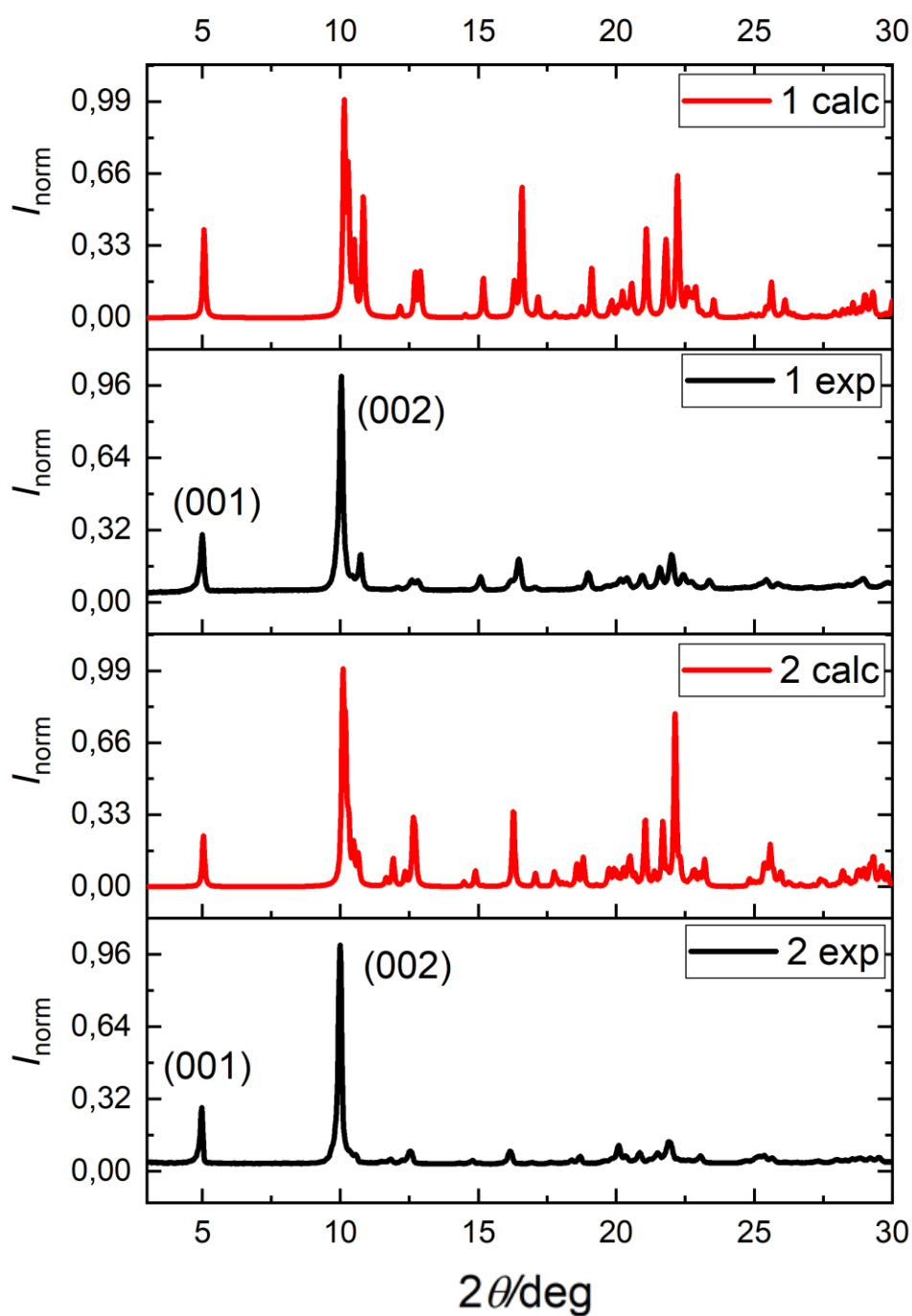


Fig. S11 XRPD data for compounds **1** and **2**. Red lines: diffraction pattern calculated from the single-crystal structure for $\lambda = 1.54056 \text{ \AA}$, Black lines: experimental data.

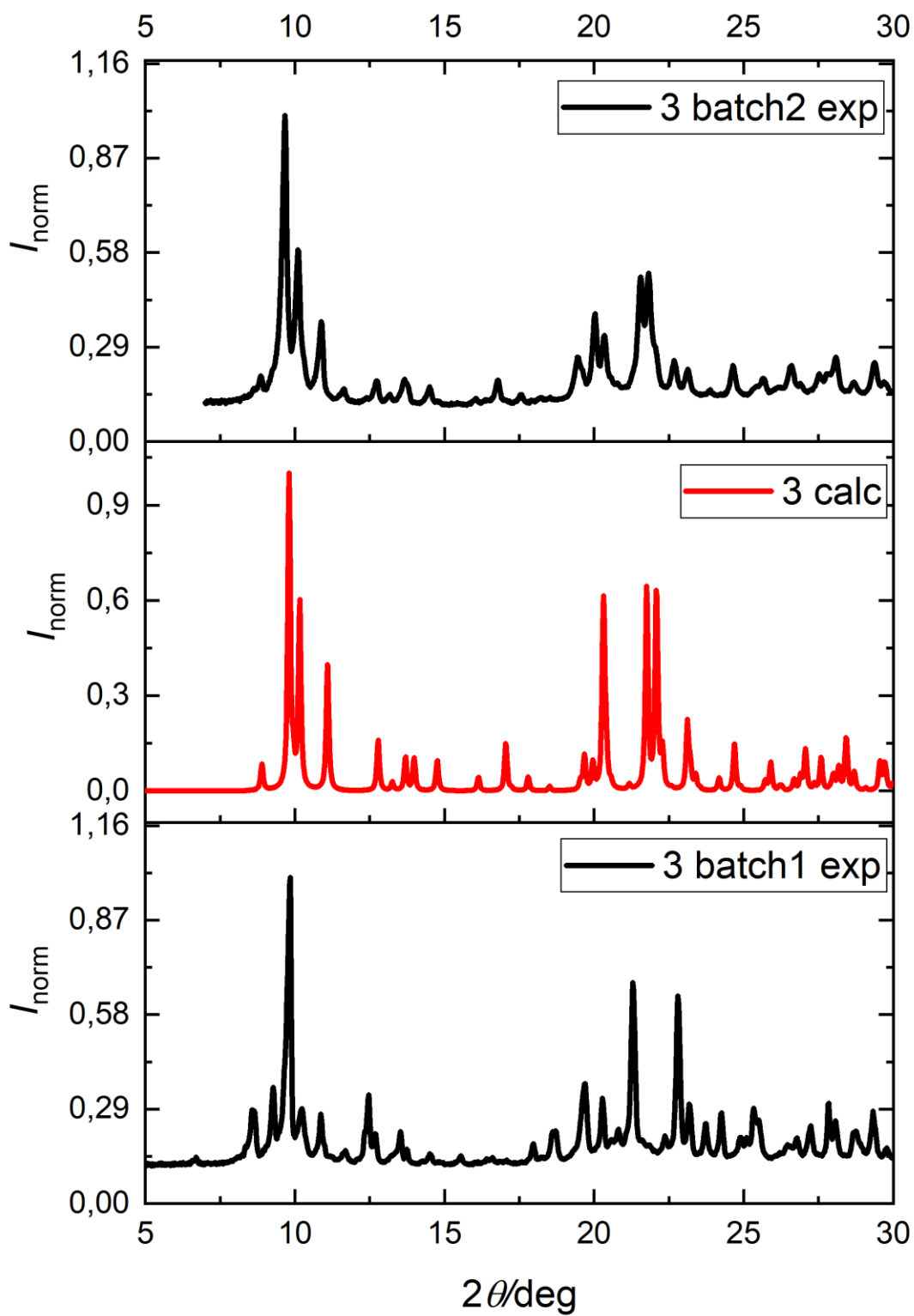


Fig. S12 XRPD data for both batches of **3**. Red lines: diffraction pattern calculated from the single-crystal structure for $\lambda = 1.54056 \text{ \AA}$, Black lines: experimental data.

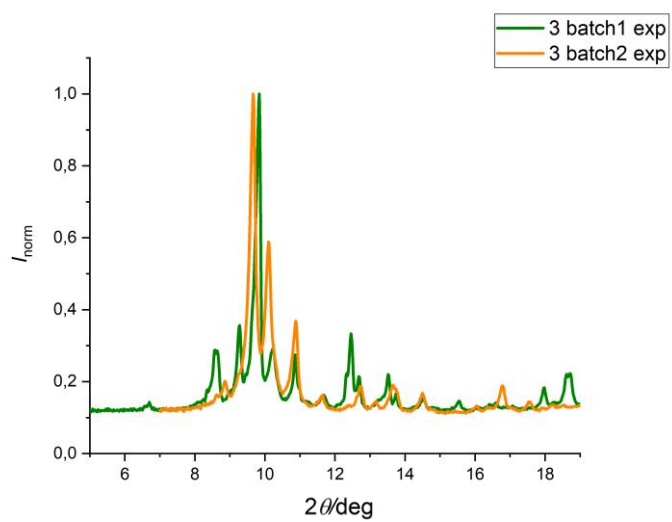
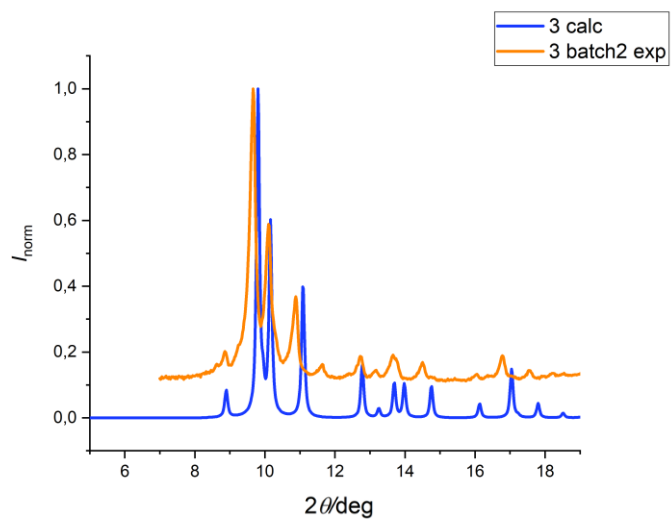
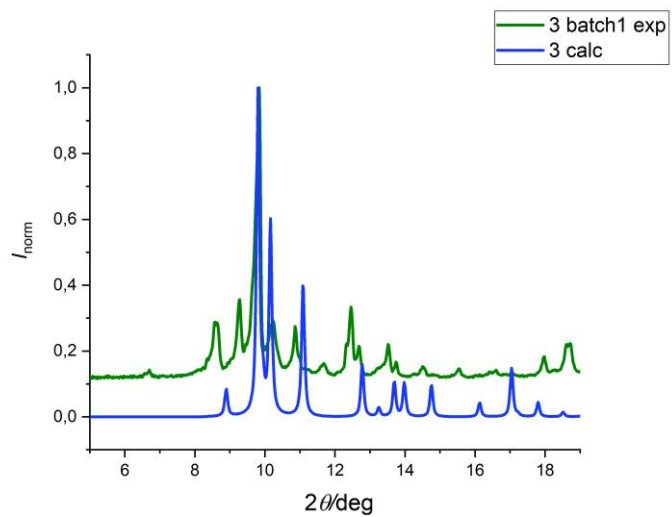


Fig. S13 Comparison of the low-angle XRPD data for both batches of **3** (batch 1 – green, batch 2 – orange) and calculated diffraction pattern (blue).

Supporting Information References

- ¹ B. Corain, B. Longato, G. Favero, D. Ajò, G. Pilloni, U. Russo and F. R. Kreissl, *Inorg. Chim. Acta*, 1989, **157**, 259–266.
- ² M. M. Rohmer, A. Veillard and M. H. Wood, *Chem. Phys. Lett.*, 1974, **29**, 466–468.
- ³ M. B. Casu, C. Tönshoff, H. F. Bettinger, S. Schundelmeier, S. Abb, S.-A. Savu and T. Chassé, *RSC Adv.*, 2012, **2**, 5112.
- ⁴ S. A. Savu, I. Biswas, L. Sorace, M. Mannini, D. Rovai, A. Caneschi, T. Chassé and M. B. Casu, *Chem. - A Eur. J.*, 2013, **19**, 3445–3450.
- ⁵ A. B. Fischer, M. S. Wrighton, M. Umana and R. W. Murray, *J. Am. Chem. Soc.*, 1979, **101**, 3442–3446.
- ⁶ P. G. Gassman, D. W. Macomber and J. W. Hersberger, *Organometallics*, 1983, **2**, 1470–1472.
- ⁷ C. M. Woodbridge, D. L. Pugmire, R. C. Johnson, N. M. Boag and M. A. Langell, *J. Phys. Chem. B*, 2000, **104**, 3085–3093.
- ⁸ A. Rosencwaig, G. K. Wertheim and H. J. Guggenheim, *Phys. Rev. Lett.*, 1971, **27**, 479–481.
- ⁹ D. C. Frost, C. A. McDowell and I. S. Woolsey, *Chem. Phys. Lett.*, 1972, **17**, 320–323.
- ¹⁰ D. G. Brown and U. Weser, *Zeitschrift für Naturforsch. - Sect. B J. Chem. Sci.*, 1979, **34**, 1468–1470.
- ¹¹ G. Poneti, M. Mannini, B. Cortigiani, L. Poggini, L. Sorace, E. Otero, P. Sainctavit, R. Sessoli and A. Dei, *Inorg. Chem.*, 2013, **52**, 11798–11805.
- ¹² H. S. O. Chan, T. S. Andy Hor, L.-T. Phang and K. L. Tan, *J. Organomet. Chem.*, 1991, **407**, 353–357.
- ¹³ J. K. Kouba, J. L. Pierce and R. A. Walton, *J. Organomet. Chem.*, 1980, **202**, C105–C107.
- ¹⁴ M. Barber, J. A. Connor, L. M. R. Derrick, M. B. Hall and I. H. Hillier, *J. Chem. Soc., Faraday Trans. 2*, 1973, **69**, 559–562.
- ¹⁵ A. Karam, R. Tenia, M. Martínez, F. López-Linares, C. Albano, A. Diaz-Barrios, Y. Sánchez, E. Catarí, E. Casas, S. Pekerar and A. Albornoz, *J. Mol. Catal. A Chem.*, 2007, **265**, 127–132.
- ¹⁶ A. R. Karam, E. L. Catarí, F. López-Linares, G. Agrifoglio, C. L. Albano, A. Díaz-Barrios, T. E. Lehmann, S. V. Pekerar, L. A. Albornoz, R. Atencio, T. González, H. B. Ortega and P. Joskowics, *Appl. Catal. A Gen.*, 2005, **280**, 165–173.